frontiers | Frontiers in Geochemistry

TYPE Original Research
PUBLISHED 01 November 2023
DOI 10.3389/fgeoc.2023.1244283

OPEN ACCESS

EDITED BY
Yiliang Li,
The University of Hong Kong, Hong Kong SAR, China

REVIEWED BY
Alsu Kuznetsova,
University of Alberta, Canada
Richard Wilkin,
U.S. Environmental Protection Agency, United States
Si Sun,
China University of Geosciences Wuhan, China

*CORRESPONDENCE
Marc Tamisier,
marc.tamisier@ufz.de

RECEIVED 22 June 2023
ACCEPTED 28 September 2023
PUBLISHED 01 November 2023

CITATION
Tamisier M, Musat F, Richnow H-H, Vogt C and Schmidt M (2023), On the corrosion of ductile cast iron by sulphate reducing bacteria—implications for long-term nuclear waste repositories. *Front. Geochem.* 1:1244283. doi: 10.3389/fgeoc.2023.1244283

On the corrosion of ductile cast iron by sulphate reducing bacteria—implications for long-term nuclear waste repositories

Marc Tamisier[1]*, Florin Musat[1,2,3], Hans-Hermann Richnow[1,4], Carsten Vogt[1] and Matthias Schmidt[1]

[1]Department of Isotope Biogeochemistry, Helmholtz-Centre for Environmental Research–UFZ, Leipzig, Germany, [2]Department of Molecular Biology and Biotechnology, Faculty of Biology and Geology, Babeş-Bolyai University, Cluj-Napoca, Romania, [3]Department of Biology, Section for Microbiology, Aarhus University, Aarhus, Denmark, [4]Isodetect Umweltmonitoring GmbH, Leipzig, Germany

Ductile cast iron is a candidate material for long term nuclear waste repository canisters. However, little is known about microbial corrosion of this material, a phenomenon threatening the integrity of the repository. Here, the corrosion of ductile cast iron (92.73%–94.19% Fe) and mild steel (~99.37% Fe) by the sulphate reducing bacterium *Desulfopila corrodens* were compared. Particular attention was payed to the impact of graphite nodules in ductile cast iron on the corrosion. The two materials developed similar crusts after 36 days. However, in the early corrosion stages different mineral compositions of the formed crusts were observed, e.g., dome shaped minerals (<1 µm) that formed on mild steel were absent on ductile cast iron. Further, iron sulphide was formed equally on all surfaces, the iron and graphite nodules. Our results contribute to the understanding of how microbial activity drives the corrosion of ductile cast iron made structures (e.g., canisters) in long-term nuclear waste repositories, particularly with respect to the mineral composition of the crust at different stages of the corrosion process. We propose that under the conditions used in this study, the ductile cast iron and mild steel bio-corrode similarly on long time scales which makes both material not favourable for use in long term nuclear waste repository with regard to microbial corrosion.

KEYWORDS

microbially influenced corrosion, sulphate reducing bacteria, *Desulfopila corrodens*, IS4, biomineralisation, long-term nuclear waste repository, ductile cast iron, mild steel

Introduction

Numerous countries worldwide produce energy from nuclear fission power plants, a technology relying on nuclear fission that generates radioactive waste. Some of the waste is classified as high-level waste (HLW) and will have to be stored for hundreds of thousands of years to reach a non-threatening degree of radioactivity for the human beings (Deng et al., 2020). Thus, concepts to store these wastes have to ensure an integrity over hundreds of thousands of years.

Worldwide, concepts of storing nuclear waste in deep geological strata has been developed during the past decades. Different geological formations, such as salt caverns (Langer, 1999), Opalinus clay or crystalline rocks, are considered as candidates for such repositories (Kim et al., 2011; Birkholzer et al., 2012). Also, different types of metals like

ductile cast iron, copper or titanium as well as metal alloys, e.g., nickel based, have been studied as potential canister materials for the different repository concepts (King, 2017). In order to establish a mechanical barrier between the canister and the host rock, the canisters would then be imbedded in highly compacted bentonite (Smith et al., 2014).

One of the crucial parameters concerning the integrity of a nuclear waste repository is the potential corrosion of the canisters which will occur via different mechanisms during the entire life time of the repository (Zhang et al., 2019). Corrosion of the canisters may be strongly enhanced by the activity of microbes. On the one hand, this may occur by the production and release of oxidative molecules, a process which is named chemical microbiologically influenced corrosion (CMIC) (Enning and Garrelfs, 2014). On the other hand, some microorganisms have the capacity to induce corrosion by taking up electrons directly from the metal, a process referred to as electrical microbiologically influenced corrosion (EMIC) (Enning and Garrelfs, 2014).

In geological formations considered for nuclear waste repository, for example, the Opalinus clays, the presence of sulphate reducing bacteria (SRB) has been observed and considered as a possible corrosive threat (Bagnoud et al., 2016). Also, SRBs have been found in the clay rock and in bentonite (Masurat et al., 2010a; Engel et al., 2019). Potentially, the metal of the canisters can serve as electron donor for microbial sulphate reduction, according to reaction 1 (Enning et al., 2012):

$$4\,Fe\,(0) + SO_4^{2-} + 3\,HCO_3^- + H_2O \;\text{->}\; FeS + 3\,FeCO_3 + 5\,HO^- \quad (1)$$

With the $\Delta G^0 = -46.8$ kJ/mol Fe, calculated considering standard state.

Alternatively, Fe(0) may be indirectly biocorroded by the generated sulphide according to reaction 2 (Enning et al., 2012):

$$Fe\,(0) + H_2S \;\text{->}\; FeS + H_2 \quad (2)$$

With the $\Delta G^0 = -72.3$ kJ/mol. The calculation of the for equation 1 and 2 are shown in the material and methods section.

Notably, the formation of FeS in the presence of SRBs and Fe (0) is not limited to nuclear waste repositories but is relevant for many systems with iron-based man-made infrastructure and has also been observed in ground water (Gu et al., 2002) and marine systems (Enning et al., 2012).

The presence of compacted bentonite largely suppresses microbial metabolic activities due to the combination of low water activity (intended to be below 0.96) and high swelling pressure (intended to be greater than 2 MPa) (Masurat et al., 2010a; Stroes-Gascoyne et al., 2010; Stroes-Gascoyne et al., 2011). However, compacted bentonite does not eliminate the presence of microorganisms. Furthermore, potential local decompaction of the bentonite, for instance due to its expansion at placement gaps or because of bentonite losses at the bentonite/rock interface caused by water-carrying fractures, is likely to provide conditions where microbial growth takes place (Masurat et al., 2010; Stroes-Gascoyne et al., 2011).

In order to estimate the potential of corrosion influenced by microorganisms and more specifically by SRBs in the context of long-term nuclear waste repositories, it is important to characterise the susceptibility of candidate cask materials to MIC, as well as the way microbes interact with them.

Ductile cast irons (DCI) are considered candidate materials for canisters for long term nuclear waste repositories in Germany (GNS. 2023). Compared with steel, DCI offers advantageous mechanical and casting properties due to its heterogeneity caused by the presence of spherical graphite nodules (Iacoviello et al., 2018). The potential impact of the graphite nodules on MIC processes is currently unknown.

Here we tested the susceptibility of ductile cast iron to corrosive microorganisms, and how chemical composition of the material, particularly the presence of graphite nodules, impact MIC. For this purpose, we used the corrosive sulphate reducing bacterium *Desulfopila corrodens* strain IS4, known to be highly corrosive and able to perform both, EMIC and CMIC (Dinh et al., 2004; Enning et al., 2012). *D. corrodens* was cultured in artificial sea water under conditions less complex than the bentonite environment in which the cask will be embedded. These conditions might be optimal for the activity of *D. corrodens* and do not mimic the conditions in the waste repository but will allow to investigate on how the iron-based materials is affected by the MIC process. Furthermore, the selected experimental conditions enabling considerable activity of *D. corrodens* permitted to study the behavior of ductile cast iron while facing severe MIC in a short time, and thus resembled a worth case scenario for MIC. The strain was incubated with coupons of DCI or mild steel (99.37% Fe) as sole sources of reducing equivalents. The resulting corrosion process was characterised with respect to formation of corrosion crust structures on the iron surface, and the potential impact of the DCI graphite nodules on the formation of such structures. The crusts were analysed structurally by scanning electron microscopy (SEM) and the elemental composition was analysed by energy dispersive X-ray spectroscopy (EDX) with the aim to determine a potential correlation between the elemental composition repartition on the coupon surface and observed features of the materials. Finally, chemical analysis was performed by Raman-micro-spectroscopy in order to determine the mineral composition of the corrosion crusts.

Material and methods

Strain, culturing conditions

The sulphate reducing bacterium *D. corrodens* strain IS4 was grown in anoxic artificial see water (ASW) as described previously (Dinh et al., 2004). The medium contained (mM): NaCl, (451); $MgCl_2 \cdot 6\,H_2O$, (28); $CaCl_2 \cdot 2\,H_2O$, (10.1); KCl, (8.9); KBr, (0.8); NH_4Cl, (0.0037); KH_2PO_4, (0.0011); $MgSO_4 \cdot 7\,H_2O$, (28). $NaHCO_3$ (30 mM) was used to buffer the medium. The medium was reduced with Na_2S (1 mM) and Na dithionite (0.17 mM). Trace elements and vitamins were added according to Widdel (2010). The pH of the medium ranged between 7.0 and 7.3. Preparation of anoxic culture media was done following established protocols (Laso-Perez et al., 2018).

D. corrodens IS4 was routinely grown autotrophically with H_2 as electron source and sulphate as electron acceptor. Cultures were established in 120 mL serum bottles containing 45 mL of ASW medium under a headspace of N_2/CO_2 (9/1, v/v), and inoculated with 5 mL of a grown culture. H_2 was added to the headspace at 1 bar partial pressure. When H_2-grown cultures produced about 4 mM

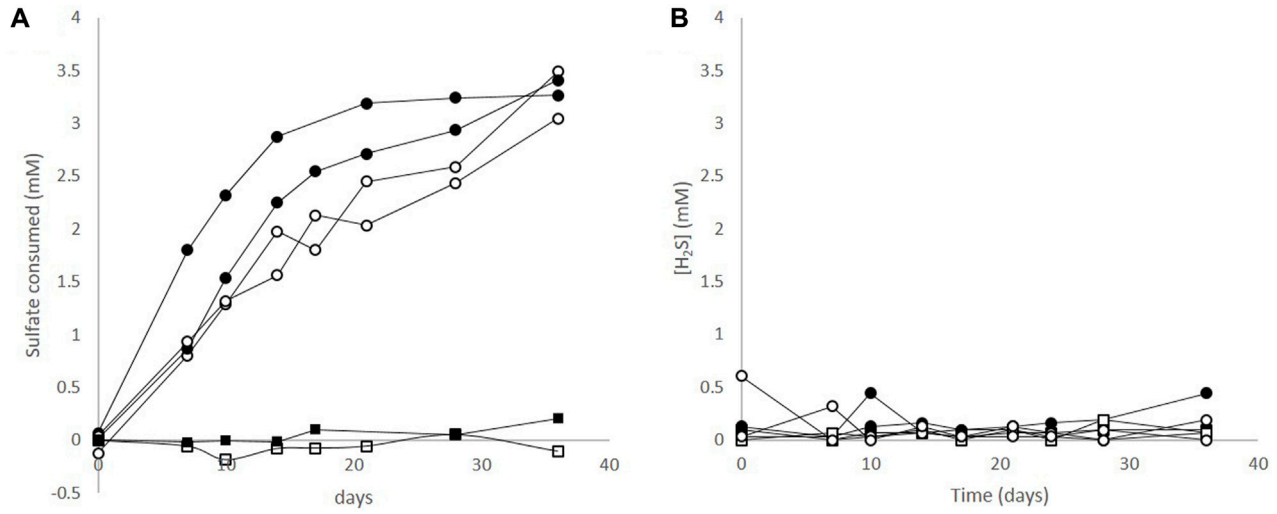

FIGURE 1
Sulphate and sulphide profiles during corrosive growth of the sulphate reducing bacterium *Desulfopila corrodens* strain IS4. **(A)** Sulphate consumption in cultures of strain IS4 with ductile cast iron (●), and with mild steel (○). No sulphate was consumed in abiotic controls with ductile cast Iron (■), or mild steel (□) **(B)** Sulphide concentrations in cultures of *Desulfopila corrodens* strain IS4 with ductile cast iron (●), and mild steel (○), and in corresponding abiotic controls, (■,□).

sulphide, 5 mL were used to inoculate replicate cultures provided with iron coupons as the sole electron source (Supplementary Table S1). Coupons of mild steel (EN 1.0330[1]; >99.37% Fe; 5 cm long, 1 cm width, 1 mm thick), or ductile cast iron (EN-GJS400-15C, EN16482[2]; 5 cm long, 1 cm width, 2 mm thick) were used (1 coupon per culture). The cultures were sealed using butyl-rubber stoppers and incubated at 28°C with shaking at 100 rpm within an incubator (Gesellschaft für Labortechnik mbH (GFL) typ 3032, Burgwedel/Germany). Abiotic controls consisted of steel or DCI coupons in 50 mL sterile ASW medium, and were prepared following the same procedures.

Analytical methods

For sulphide concentration measurements, volumes of 0.1 mL were withdrawn from cultures with N_2-flushed syringes and mixed with 4 mL of a Cu_2SO_4 (5 mM) solution in 50 mM HCl in MQ water. The absorbance of the generated colloidal CuS was measured photometrically at 480 nm. The relation between the sulphide concentration and the optical absorbance of the CuS solution is linear and thus the sulphide concentration was calculated based on the CuS solution absorbance (Cord-Ruwisch, 1985). To determine sulphate concentrations, 0.1 mL culture, collected with N_2-flushed syringes, were diluted 20-fold in deionised water and filtered through 0.22 µm pore-size filters (PES 100pk green, Restek). Sulphate concentration were measured by ion chromatography (ICS 5000, Thermo Fisher Scientific) equipped with an AS11-HC column (Thermo Fischer Scientific) and a Dionex EGC III KOH eluent generator cartridge (Thermo Fisher Scientific) using an isocratic method with MQ-water as input solvent with a flow of 0.380 mL min-1 for 36 min. The obtained sulphate concentrations were normalized based on the chloride peak. Chloride can be used as an internal standard due to its high concentration not impacted by the chemical processes taking place in the culture. In dataset 2 (Supplementary Table S1), in seven out of 35 samples, chloride peaks were measured that deviated from the known chloride value by more than 10% with no known mechanistic explanations. A Rosners test (Rosner, 1975) for multiple out-layers was performed on this dataset chloride peak values. The test considered the seven samples mentioned previously as outliers and these samples were subsequently removed. Calibration was performed by using salt solutions of similar composition as the used culture media with variating sulphate concentration (7.7; 16.1; 23.9; 32 mM).

The pH was measured using a pH meter (Schott instruments). At the beginning of the experiment, the pH of the prepared medium was measured by immersion of the pH meter electrode in 3 mL of collected medium. At the end of the culture experiment, the pH was measured again by immersing the pH meter electrode directly in the serum bottle straight after removal of the steel coupon.

Sample preparation for structural and chemical imaging of corrosion crusts

For preparation of samples for microscopy, corroded coupons were chemically fixed anoxically for 16 h at 4°C with 2% glutaraldehyde prepared in anoxic ASW medium. The coupons were then rinsed in ASW medium, and dehydrated by treating in a graded ethanol series of 30% v/v (in ASW) to 50%, 70%, 90%, 95%, 100% (in pure water, v/v) (3 min incubation for each concentration). Thereafter, the coupons were incubated at room temperature in 50%

1 99.37% Fe; 0.12% C; 0.045% p; 0.045% S; 0.6% Mn.

2 92.73% - 94.19% Fe; 3.25% - 3.7% C; 2.4% - 3% Si; 0.1% - 0.4% Mn; 0.015% - 0.08% P; 0.005% - 0.02% S; 0.04% - 0.07% Mg.

(v/v) hexamethyldisilane (HMDS) in ethanol followed by pure HMDS (10 min each) and subsequently air-dried. Until analysis the coupons were stored in a desiccator under vacuum to avoid additional oxidation. When coupons were withdrawn from the culture, the cultivation was finished since pursuing the experiment with additional coupons in the culture would have generated a risk of oxygen insertion. Subsequently, each coupon analysis corresponds to a different culture experiment.

Scanning electron microscopy

Structural analysis of microbial cells and corrosion crusts was carried out with a high-resolution scanning electron microscope, SEM (Zeiss Merlin VP Compact, Carl Zeiss Microscopy, Oberkochen, Germany) using an electron acceleration voltage of 2 kV. For imaging secondary electron detection with an Everhard-Thornley-type detector was used. Elemental microanalysis was done by coupling the SEM with an energy dispersive X-ray spectrometer, EDX (Bruker Quantax X-Flash, Bruker Nano GmbH) using an electron acceleration voltage of 18 kV at a beam current of about 250 pA.

Raman micro-spectroscopy

The mineralogy of the corrosion crust was analyzed using a confocal Raman microscope (WiTec alpha300Ra, WiTec Wissenschaftliche Instrumente und Technologie GmbH). For excitation, a frequency doubled 532 nm solid-state laser with a laser power of 1.2 mV was used. The exposure time was set to 10 s with 50 spectra accumulated per analysis. The Raman spectra were acquired with a Peltier-cooled CCD detector attached to a grating monochromator (600 g/mm centered at 602 nm).

Standard Gibbs energy calculation

The ΔG^0 were calculated as followed:

$$\Delta G^0 = \Sigma \Delta G_f^{\ 0}(\text{products}) - \Sigma \Delta G_f^{\ 0}(\text{educts})$$

The Gibbs energy of formation used are listed in Supplementary Table S3 (Ayala-Luis et al., 2008; Azoulay et al., 2012; Bénézeth et al., 2009; GNS, 2023; Hua and Li, 2011; Masurat et al., 2010b; Ning et al., 2014; Simonov and Likholobov, 2003).

Results

Microbiologically influenced corrosion monitoring via development of sulphate, sulphide concentrations and the pH values

Microbial metabolic (corrosive) activity was monitored by measuring sulphate consumption, sulphide formation, and changes in pH during incubation.

After 36 days of incubation with ductile cast iron or mild steel, up to 3.5 mM of the added sulphate had been consumed which corresponds to an theoretical oxidation of 14 mM of Fe(0) (reaction 1, Figure 1, Supplementary Figure S1) and a loss of less than 1% of the coupon initial mass. During the same incubation time, sulphide concentrations remained constant (Figure 1, Supplementary Figure S1), thus an electron balance based on the formation of dissolved sulphide could not be calculated. In the abiotic controls, sulphate consumption and sulphide production were not observed. During the course of the incubations, the pH increased from 7.0 to 7.3 to 8.3 ± 0.13 at the end of the experiment in the microbial corrosion cultures with both materials. Indeed, the microbial corrosion process is producing HO^- and consuming the carbonate buffer leading to the observed pH increase. In the abiotic controls, the pH at the end of the experiment was 7.7 ± 0.23.

Micro-analysis of the corrosion crust

In order to investigate the micro topography and elemental composition of the corrosion crust, SEM and EDX analyses were performed after different periods of incubation.

After 36 days of corrosion by *D. corrodens*, both types of coupons, ductile cast iron and mild steel, were entirely covered with an ochre to dark brown coloured crust. Similar structures have been formerly observed with mild steel, albeit after sensibly longer incubation times (Enning et al., 2012). SEM surface analysis of the crust showed cells of *D. corrodens* on the corroded surfaces of both types of coupons (Figure 2). Structurally, the crust appeared similar for both the ductile cast iron and the mild steel. For the mild steel, it can be compared to the structures founds in SEM analysis performed after 3 months of corrosion by strain IS4 (Enning et al., 2012) or the structures formed on a pure iron electrode corroded by strain IS4 for 6 weeks (Venzlaff et al., 2013). Unlike previous studies with strain IS4, here dome shaped minerals were present in low abundance or absent depending on the replicate; instead, rectangular shaped mineral structures were observed (Figure 2; Enning et al., 2012; Venzlaff et al., 2013). A subsequent analysis of the crust for both ductile cast iron and the mild steel by EDX revealed that the crust was mainly composed of C, O, P, S, Mg, Ca and Fe (only those detectable by EDX), with C and O being omnipresent. On both types of coupons, the presence of differently composed minerals was observed with regard to their elemental composition, namely, sulphides (Fe/S and Ca/Fe/S), and phosphates (Ca/P and Mg/P). Also, minerals containing colocalised Ca and Fe but no S were found (Figure 2). In the abiotic controls, only some precipitations from the medium, mainly composed of Mg and P or Ca were found after 36 days of incubation. Thus, we assume that these structures were formed chemically in the reduced medium.

In order to gain deeper insight into the crust formation dynamics, a time-resolved experiment was performed in which samples were analyzed at day 2, 4, and 6 after inoculation. For ductile cast iron, the formation of a crust covering the coupons was observed already within the first 6 days of incubation. As expected, the thickness of the crust and the coverage of the coupon appeared to increase over time. In comparison, on the corroded mild steel, similar observations were made but the proportion of the coupon covered by the crust was evolving slower and with a higher variability (Figure 3). In the abiotic control experiments, no comparable crusts were observed proving that *D. corrodens* was responsible of the crust formation (data not shown).

10.3389/fgeoc.2023.1244283

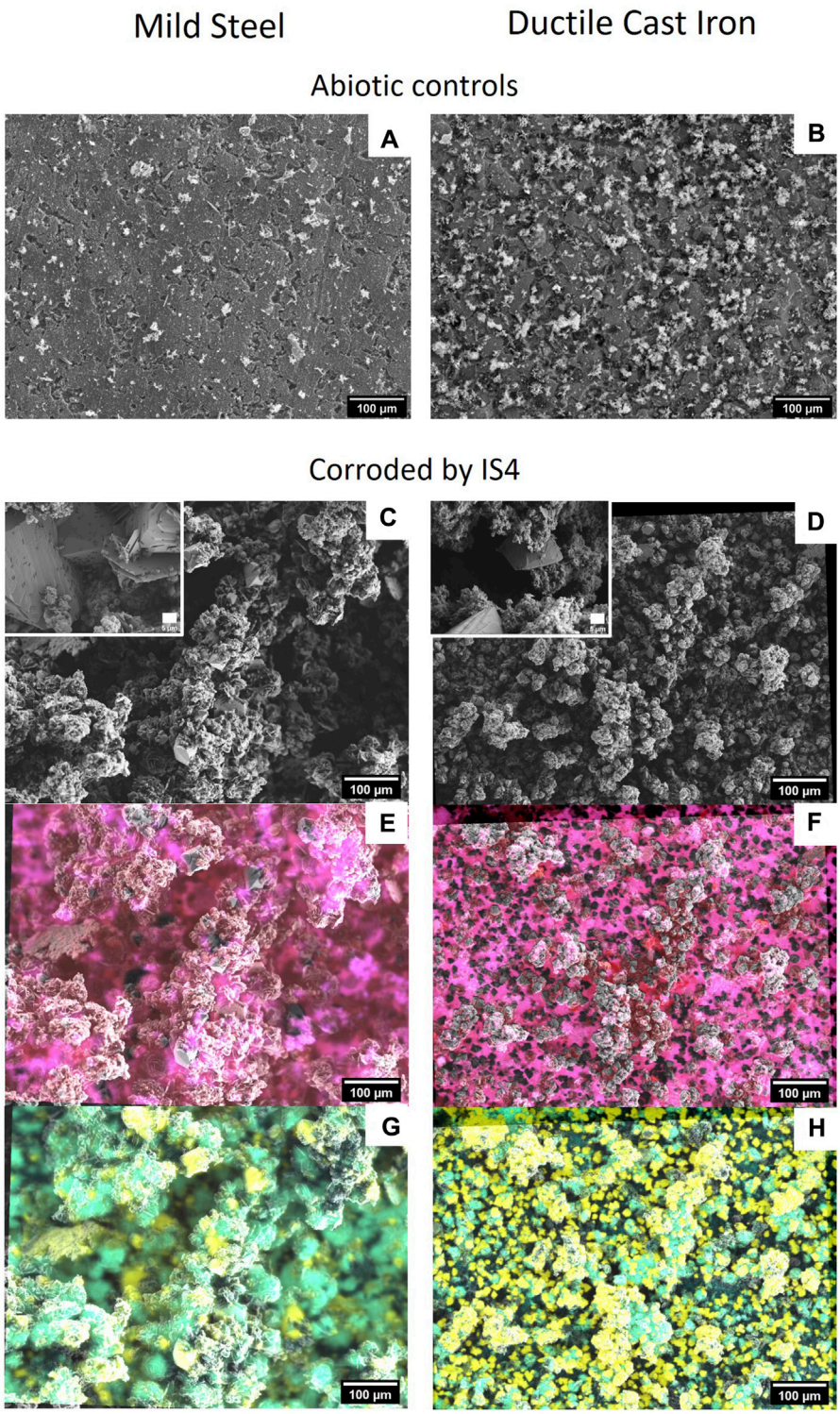

FIGURE 2
Structural and elemental composition of corrosion crusts. SEM images (2 kV) of mild steel **(C)** and ductile cast iron **(D)** corroded by strain IS4 after 36 days incubation, and abiotic controls incubated for the same time **(A)** for the mild steel and **(B)** for the ductile cast iron). **(E)** correspond to EDX at 18 kV with overlay of iron (red) and sulphur (blue) (pink = co-occurrence of iron and sulphur) for mild steel corroded by IS4 after 36 days and **(F)** is the equivalent for the ductile cast iron. **(G)** correspond to EDX at 18 kV with overlay of calcium (yellow) and phosphorous (light blue) (green = co-occurrence of calcium and phosphorus) for the mild steel corroded by IS4 after 36 days and **(H)** is the equivalent for the ductile cast iron.

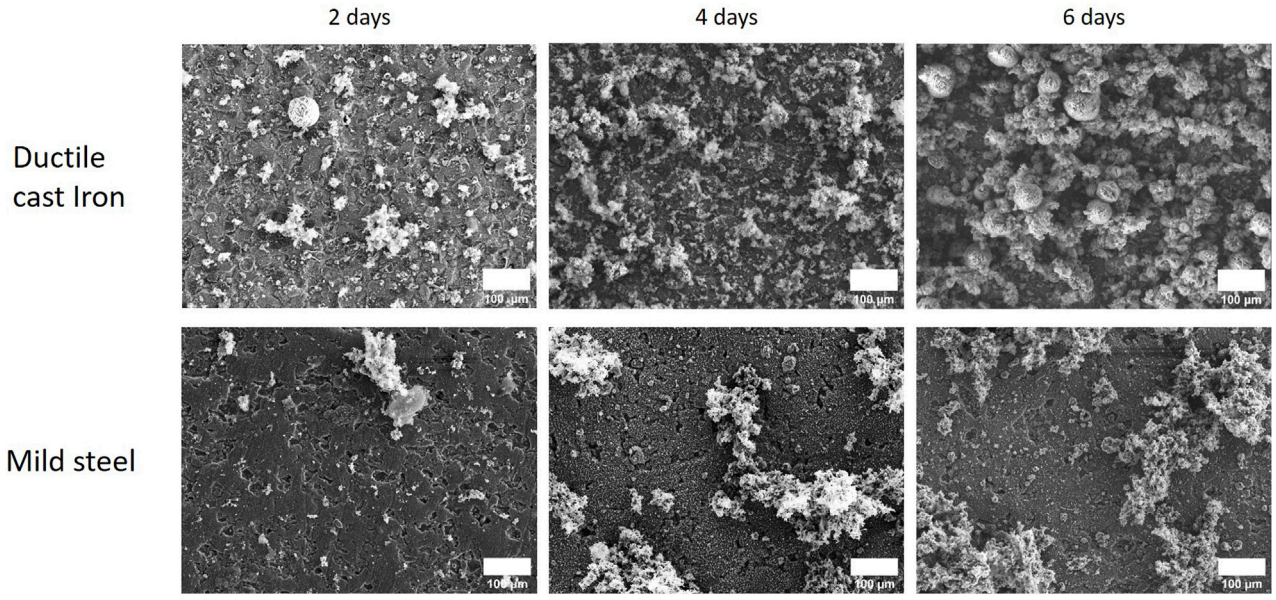

FIGURE 3
Time-resolved experiment showing the dynamics of corrosion crust formation by strain IS4 with mild steel and ductile cast iron. SEM images (18 kV) of the ductile cast iron and mild steel corroded by the sulphate reducer strain IS4 after 2, 4 and 6 days of incubation.

Ductile cast iron

Notably, the structural analysis of the crust on ductile cast iron coupons revealed no patterns structurally associated with the graphite nodules (darker patches in Figure 3, DCI 2 days). In order to detect changes in its elemental composition, the corrosion crusts were analysed by SEM-EDX and the relative abundances of S, Fe, Ca and C were quantified. Thereby, it was found that in the ductile cast iron samples, the relative abundance of sulphur on the surface of the coupon did not vary in correlation with the presence of the graphite patches. In the abiotic controls, in contrast, the distribution of sulphur, resulting from the presence of sulphide in the media as reductive agent, appeared nonhomogeneously distributed for both ductile cast iron and mild steel. A correlation with the presence of graphite nodules could be determined since the sulphur signals were lower on the graphite surfaces (Supplementary Figure S2). For calcium, a correlation could be found at early corrosion stages (2 days) in the microbial corrosion experiment and the abiotic controls. Here, calcium was found to be located only on the iron surfaces but never on the graphite patches (Figure 4).

Mild steel

The corrosion crust resembled very much those formed on ductile cast iron but, in addition, small dome-shaped minerals (<1 µm) were found. Sometimes, these minerals were located on the surface of microbial cells, leading to cell incrustation, but mainly, they were scattered on the surface of the coupon with a varying distribution across the different replicates (Figure 5). With regard to the elemental composition of the crust formed on mild steel, it was similar to the one observed on ductile cast iron but with an apparently lower EDX signal of sulphur which on top of that strongly varies for different locations on the surface. A correlation to P, Mg and Ca was found as areas with stronger sulphur signal typically also showed stronger P, Mg and Ca signals but lower EDX signals of iron (Figure 4).

In some cases, the dome shaped minerals formed larger aggregates having the appearance of microbial cells. The analysis of these cell-shaped minerals by SEM-EDX using an electron energy of 18 kV allowed to analyse deeper sections in the crust. The interior of this type of mineral structures was electrically charging under the electron beam, yielded low iron and sulphur signals in the EDX spectrum (Supplementary Figure S3) and often assumed a shape similar to *D. corrodens* cells suggesting that *D. corrodens* were incrusted during MIC.

Microbial cells were observed on both mild steel and ductile cast iron within 6 days of corrosion. Their location did not appear to correlate with material specific features such as cracks or graphite nodules.

Chemical analysis of the crust

The Raman micro-spectroscopy analysis on coupons corroded by *D. corrodens* for more than 36 days is presented in Figure 6. Three types of spectra were common to ductile cast iron and mild steel while one type of spectrum was only observed in the experiments with the mild steel (Figure 6; Supplementary Figure S4). The spectra demonstrated the presence of mineral mixtures (Figure 6; Table 1). A clear signature for carbonate minerals were present (bands at 1,085/1,105 cm^{-1}).

Discussion

The corrosion of a ductile cast iron and a mild steel induced by the sulphate reducing strain *D. corrodens* was investigated and

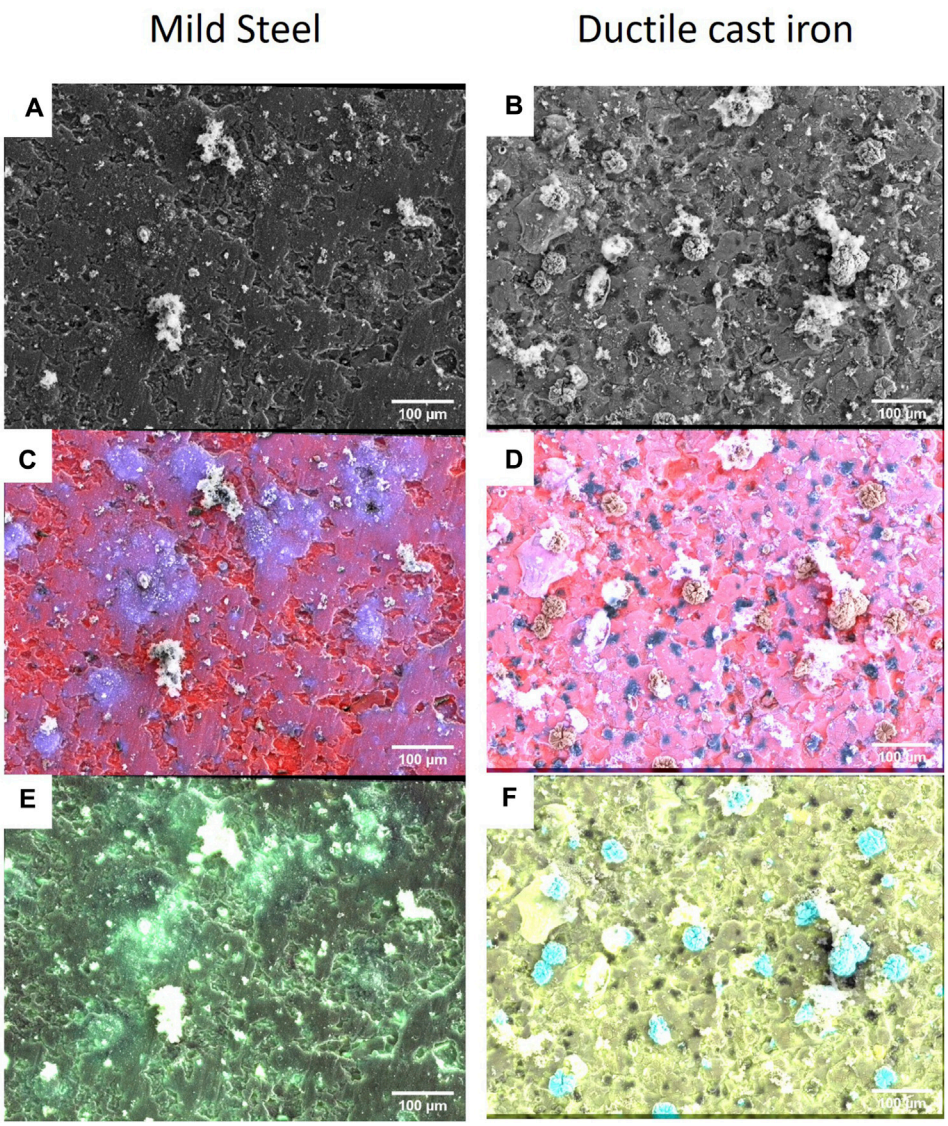

FIGURE 4
Ductile cast iron and mild steel corroded by the sulphate reducer strain IS4 for 2 days. SEM images at 18 kV for the mild steel **(A)** and the ductile cast iron **(B)** and SEM-EDX at 18 kV with overlay of iron (red) and sulphur (blue) (pink = co-occurrence of iron and sulphur) for the mild steel **(C)** or the ductile cast iron **(D)**, overlay of calcium (yellow) and phosphorous (light blue) (green = co-occurrence of calcium and phosphate) in the case of the mild steel **(E)** or ductile cast iron **(F)**. Abiotic conditions are presented in Supplementary Figure S2.

compared with regard to corrosion kinetics and crust formation. To investigate the kinetics of the microbial corrosion, the consumption of sulphate in the system was monitored. Indeed, in such system, the sulphur and iron balances are difficult to achieve due to formation of soluble species and precipitates, thus, the consumption of sulphate can be used as a proxy to quantify the amount of oxidised iron, since sulphate is usually reduced to sulphide without accumulation of intermediates by sulphate reducers (Rabus et al., 2015). As expected, the strain corroded both types of iron material and reduced sulphate to sulphide. *D. corrodens* is capable to withdraw electrons for sulphate reduction from Fe(0) thereby releasing Fe(II) cations (Enning et al., 2012). Fe(II) is water soluble but will subsequently react with the produced sulphide to form iron sulphide (FeS) (Reaction 1; Enning et al., 2012). This is supported by the EDX data acquired on the crust (Figure 2). According to Reaction 1, Fe(II) is expected to be present in fourfold excess compared to sulphide and will capture dissolved sulphides to form FeS which mainly precipitates directly at the corroded iron surface. Fe(II) is further present to form iron carbonates, i.e., siderite ($FeCO_3$) as the end-member of (Mg, Ca, Fe)CO_3 carbonates. The sulphide mineral that forms directly on the iron surface in the early stage by sulphate reducing bacteria induced corrosion is mackinawite (FeS). Indeed, it is the first mineral formed in the reaction of Fe(II) with sulphide (Csákberényi-Malasics et al., 2012; Rickard, 2014). This mackinawite forms a dark, brownish precipitate (Rickard, 2014) such as observed in our samples. A corrosion crust composed of FeS and siderite plus other carbonate minerals such as $CaCO_3$ has previously been observed on the mild steel while corroded by *D. corrodens* using X-ray diffraction and inductively coupled plasma optical emission spectroscopy (ICP-OES) (Enning et al., 2012). In

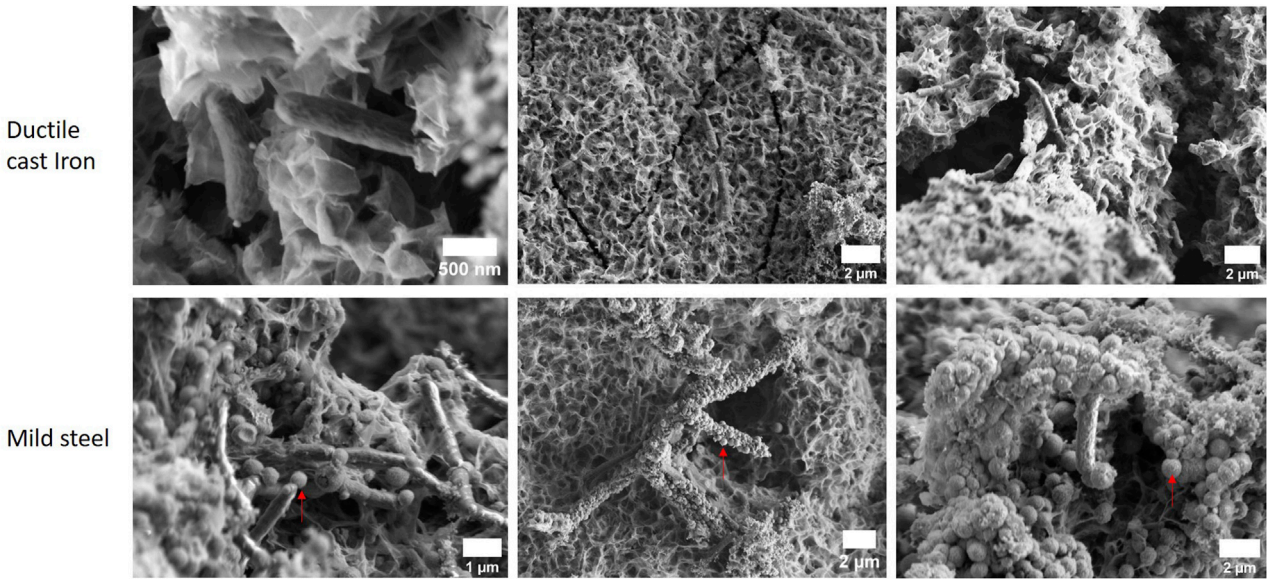

FIGURE 5
Mild steel and ductile cast iron corroded by the sulphate reducer strain IS4 within 6 days of incubation. SEM (2 kV). Red arrows indicate examples of small dome structured minerals.

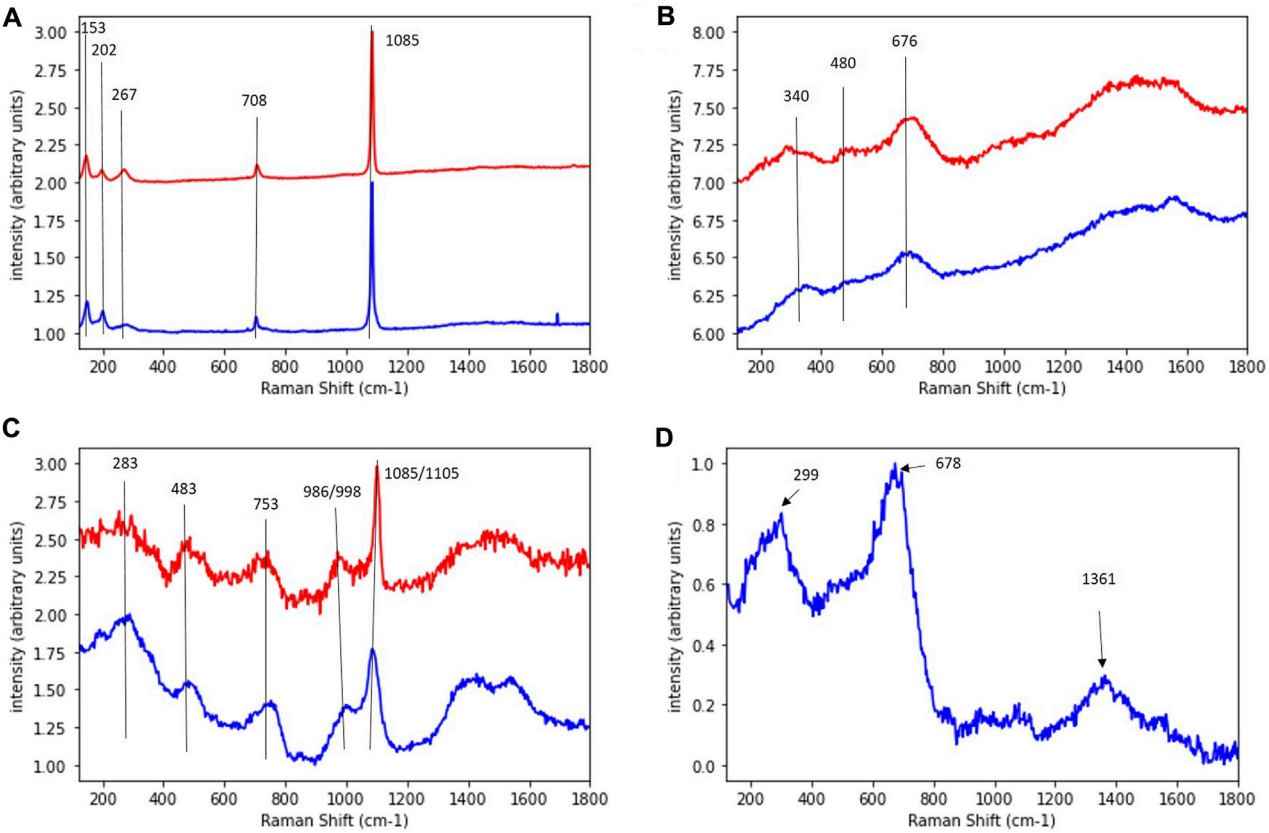

FIGURE 6
Raman spectra of the corrosion crust obtained after 36 days of corrosion by *Desulfopila corrodens* with the mild steel or the ductile cast iron. **(A–D)** represent each a different type of spectrum. Spectra corresponding to the ductile cast iron samples are presented in red and to the mild steel in blue.

TABLE 1 Comparison of spectra obtained on the corrosion crust formed after 36 days of corrosion by *Desulfopila corrodens* on the mild steel and the ductile cast iron with potential mineral present in the crust. DCI = ductile cast iron, MS = mild steel, (A), (B), (C), (D) correspond to the spectra annotation in Figure 6. 1 is set when a huge band is observed on the Raman spectrum and 0.5 when a small band is observed.

Panel A																
Lines	DCI(A)	DCI(B)	DCI(C)	MS(A)	MS(B)	MS(C)	MS (D)	Ref: Thibeau et al. (1978)			Ref: Das and Hendry, (2011)					
								Iron oxides			Iron oxide hydroxides			$Fe(CO_3)$	$NaFe_3(SO_4)_2$	
								Wüstite	Hematite	Magnetite	Goethite	Ferrihydrite	Lepidocrocite	Siderite	Na-jarosite	
150	1			1												
200	1			1										180		
218/220									222						221	
238									−230		−243					
252	1			1												
294			1			1	1		290		297		284	282	288	
307									290							
341		1			1								345			
384											384	−361	374			
396									408							
439															436	
478/480		1	1		1	1			−490		−477	−508				
518													524			
604	0.5	0.5	0.5	0.5	0.5	0.5		616	−607							
676	0.5	0.5	0.5	0.5	0.5	0.5		663		662						
698/706	1			1			1					707				
724														−722		
745			1			1										
920																
872		1			1											
961																
990			1			1										
1,033															1,008	

(Continued on following page)

10.3389/feoc.2023.1244283

TABLE 1 (*Continued*) Comparison of spectra obtained on the corrosion crust formed after 36 days of corrosion by *Desulfopila corrodens* on the mild steel and the ductile cast iron with potential mineral present in the crust. DCI = ductile cast iron, MS = mild steel, (A), (B), (C), (D) correspond to the spectra annotation in Figure 6. 1 is set when a huge band is observed on the Raman spectrum and 0.5 when a small band is observed.

Panel A															
Lines	DCI(A)	DCI(B)	DCI(C)	MS(A)	MS(B)	MS(C)	MS (D)	Ref: Thibeau et al. (1978)			Ref: Das and Hendry, (2011)				
								Iron oxides			Iron oxide hydroxides			$Fe(CO_3)$	$NaFe_3(SO_4)_2$
								Wüstite	Hematite	Magnetite	Goethite	Ferrihydrite	Lepidocrocite	Siderite	Na-jarosite
1,067												1,045		1,082	
1,085/1,104	1		1	1		1								1,082	1,105
1,361							1								
1,347															
1,434															
1,465															
1,510															
								DCI (A,B,C)						DCI (A,C)	
								MS (A,B,C)		MS (A,B,C)				MS (A,C)	

Panel B									
Ref: saheb et al. (2010)	Ref: Mernagh and Trudu (1993)				Ref: Hope et al. (2001)	ref: Remazeilles et al. (2010)		ref: Rruff database	Ref: De La Pierre et al. (2014)	
$Fe(OH)CO_3$	FeS_2					Fe_3S_4 (MIC, archeol))	FeS (MIC, archeol)	FeS	$CaCO_3$	
Chukanivite	Pyrite isotropic	Pyrite anisotropic	Pyrite	Marcasite		Greigite	Mackinawite	Troilite	Calcite	Aragonite (polycryst)
						−188	208	200		−162
238										
						−250	−253			
							283 (poor cryst)/294	280	287	283
	353	342	341	320		350				
389	387	377	379	386		365				

(Continued on following page)

10.3389/fgeoc.2023.1244283

TABLE 1 (*Continued*) Comparison of spectra obtained on the corrosion crust formed after 36 days of corrosion by *Desulfopila corrodens* on the mild steel and the ductile cast iron with potential mineral present in the crust. DCI = ductile cast iron, MS = mild steel, (A), (B), (C), (D) correspond to the spectra annotation in Figure 6. 1 is set when a huge band is observed on the Raman spectrum and 0.5 when a small band is observed.

Panel B									
Ref: saheb et al. (2010)	Ref: Mernagh and Trudu (1993)				Ref: Hope et al. (2001)	ref: Remazeilles et al. (2010)		ref: Rruff database	Ref: De La Pierre et al. (2014)	
$Fe(OH)CO_3$	FeS_2					Fe_3S_4 (MIC, archeol))	FeS (MIC, archeol)	FeS	$CaCO_3$	
Chukanivite	Pyrite isotropic	Pyrite anisotropic	Pyrite	Marcasite	Greigite	Mackinawite	Troilite	Calcite	Aragonite (polycryst)	
							390			
	−446	428	−428							
							470			
534										
672							680 (large)			
730								712	701 . . . 717	
926										
1,070								1,087	1,085	
								1,087		
								−1,437		
1,434										
1,510										
						DCI(A)			DCI (A)	
						MS(A)			MS (A)	

10.3389/fgeoc.2023.1244283

this study, Raman spectra suggesting the presence of carbonate minerals were measured on both, mild steel and ductile cast iron (Figures 6A, C). The similarity of these spectra measured on both materials further suggests a similar composition of the crust in term of carbonate minerals. Since the carbonate mineral composition of the mild steel is known from the work of Enning and coworkers (2012), we can conclude that both the crusts on mild steel and ductile cast iron are composed of siderite and calcium carbonate. The presence of chuckanovite may have been expected considering previous microbial and abiotic iron corrosion observations (Albahri et al., 2021). However, no specific indication of chukanovite was observed (Table 1). Amorphous FeS or mackinawite are difficult to identify in a heterogeneous mixture (Herbert et al., 1998) and could not be identified by Raman (Figure 6) due to the complex nature of the mineral mixtures. However, their presence had been confirmed before for the mild steel (Enning et al., 2012) and should be present for ductile cast iron as well since mackinawite is formed primarily on iron based materials corroded by SRBs (McNeil and Little, 1990). Yet, an open question that remains is the potential impact of the material being corroded on the evolution of the mineralisation forms of the iron sulphide. Overall, even though one type of Raman spectrum was only obtained on mild steel but not on ductile cast iron, Raman micro-spectroscopy demonstrated that the crusts formed on both materials present strong similarity after 36 days of corrosion under the conditions used in this study. Throughout the experiments sulphate reduction was not limited by the availability of iron, since <1% of the coupon initial mass was oxidised. Passivation of the coupons due to build-up of corrosion crusts appears unlikely, since after 36 days of incubation, the crust was conductive. Indeed, as no charging of the crust under the electron beam was observed, it can be concluded that its electrical resistance was low, probably because of the presence of FeS which is known to be electrically conductive (Venzlaff et al., 2013). In fact, even with biogeochemical processes generating solely non-conductive carbonate minerals such as iron corrosion by methanogens, a low sulphide concentration in comparison to those generated here was enough to generate a conductive crust due to the formed FeS (Tamisier et al., 2022). Also, competition between the microorganisms to access the electron source did not occur since after 36 days of incubation, the coupons surface were not densely colonised by cells to suggest such competition. The plateauing of the sulphate consumption is most likely due to the observed increase in pH (from 7.0 to 7.3 at the beginning of the incubation to 8.3 ± 0.13 at the end). Thus, an increasing pH has a detrimental effect on the kinetics of sulphate reducion. Thus, the rise of pH might have limited corrosion since an increase in pH will at term negatively affect the sulphate reduction process by SRBs (Tran et al., 2021; Gutierrez et al., 2009).

In ductile cast iron, the local microbial corrosion rate may have been influenced by the electron work functions (EWF) of the iron on the one hand and of the graphite patches on the other. Indeed, corrosion resistance is linked with the EWF and this is supported by "The higher the EWF, the higher the energy needed to remove electrons out of the metal surface and so the higher corrosion resistance" (Punburi et al., 2018, p. 2). Graphite has a EWF of 4.5–4.8 eV and iron a value of 4.31 eV. However, these values must be handled with care since typically they are measured under ultra-high vacuum conditions and are influenced by parameters such as localised electronic crystal defect states and crystalline plane orientation (Simonov et al., 2003). In addition, the work function of a material is also dependent on other properties, of particular interest here is the Young's modulus as was demonstrated for polycrystalline metals (Hua and Li, 2011). In the case of ductile cast iron, the Young's modulus is a locally varying function due to the graphite nodules (Pereira et al., 2018; Speich et al., 1980) which in turn locally impacts the EWF. These considerations raised the expectation that the graphite nodules in ductile cast iron would affect corrosion mostly at the early stages. This was indeed confirmed in the experiments: Formation of early corrosion crusts had levelled out the surface inhomogeneities in ductile cast iron such that with increasing time the overall (averaged) corrosion rate did not appear to differ significantly between ductile cast iron and mild steel (Figure 1, Supplementary Figure S1, Supplementary Table S2). When corrosion by *D. corrodens* lasted for more than 36 days, the corrosion crusts on ductile cast iron and mild steel were very similar in term of structure and elemental composition. In other words, on long time scales, the type of iron material does not appear to impact the structure of *D. corrodens* generated corrosion crust. Also, its chemical composition is mostly similar even though some differences remains as observed with the Raman analysis (Figure 6).

After 2 days of corrosion, the distribution of sulphur on the surface of the ductile cast iron coupon showed no obvious differences in intensity between the graphite nodules and the iron surface (Figure 4). If the sulphide reacts with the corrosion-generated dissolved Fe(II), which is most likely the case as explained above, the formation of FeS on the surface of the graphite nodules should not be limited by the availability of iron at these locations. Also, microbial cells locate on both, the graphite and the iron, resulting in a production of sulphide on both surfaces. This is not unexpected as cells located on graphite can extract the electrons from Fe(0) via electrical conduction since graphite is conductive. Sulphide may also diffuse along the surface of the coupon before reacting with the Fe(II) which can also serve as an explanation why after 2 days of corrosion, the sulphur signal in the EDX measurements was not significantly higher in proximity of the microbial cells.

The main differences between ductile cast iron and mild steel are, the significantly higher amount of elements other than iron in the iron phase of ductile cast iron, which is not as chemically pure as the mild steel used in this experiment (see material and methods), as well as the graphite nodules to which most likely the majority of the observed differences in the corrosion crust formation can be attributed. Thus, a comparison of the SEM-EDX analysis of the corrosion crusts on mild steel and ductile cast iron coupons incubated within the first 6 days hints to an influence of the graphite patches on the MIC process by *D. corrodens* in the case of ductile cast iron.

1) For mild steel, small (<1 μm) dome-like minerals were found (Figure 5). Interestingly, spikey minerals were regularly found on the cell surfaces which appear to act as nucleation site of the dome-like minerals (Figure 5); in several replicates they seem to be the sole location of the nucleation. The presence of microbial-cell-shaped minerals within the crust (Supplementary Figure S3) points to a incrustation of cells after mineralisation had started on the cell surfaces.

It is known that microbial cells can be nucleation sites due to the presence of negative charges on their surfaces which attract ions from the environment. The surface charge is maintained by the metabolic activity of the cells and thus generates a thermodynamically favourable environment for mineral nucleation (Hoffmann et al., 2021).

2) In the case of ductile cast iron, in contrast to mild steel, no encrusted cells whose surfaces could act as nucleation sites were found at all after 6 days of incubation. Generally, it appears, that the surface of ductile cast iron is not favourable for this mineral nucleation, as also no dome-like minerals were detected. As the graphite nodules are the strongest difference between mild steel and ductile cast iron, it is very likely that their presence or absence plays a major role in the crust formation during the early stage of MIC. This indicates that the graphite nodules locally modulate the potential for nucleation of the small dome shaped minerals on the surface of the material.

Conclusion

Ductile cast iron is a candidate material for long term nuclear waste repository canisters. Here, it was observed that when Fe(II) is in excess in the environment, FeS resulting from the activity of SRBs forms on the surface of the ductile cast iron without being influenced by the graphite patches. It suggests that the graphite incrustation will not influence the formation and deposition of FeS layers on the canisters if the Fe(II) resulting from the canister corrosion concentrate in the surrounding bentonite. In addition, it was demonstrated that even if ductile cast iron differs to the mild steel with regards to the formation of the corrosion crust at early corrosion stages, the crust is evolving toward more similarity in comparison to the mild steel at later corrosion stages. Indeed, structural aspects of the crust and elemental distribution do not differ significantly after 36 days of corrosion, only some minor mineral composition differences seem to remain as observed with the Raman-microspectroscopy. In a long-term nuclear waste repository, where long time scales are regarded, MIC evolution can thus be approximated as similar for the ductile cast iron and the mild steel.

Data availability statement

The raw data supporting the conclusions of this articles will be made available by the authors, without undue reservation on https://www.ufz.de/drp.

Author contributions

MT was involved in the experimental design, the data collection and interpretation as well as the manuscript writing. FM, H-HR, and CV provided input on the data interpretation and manuscript revision. MS participated in the experimental design, data interpretation, provided technical support and was involved in the manuscript writing. All authors contributed to the article and approved the submitted version.

Funding

The presented work was supported by the German Federal Ministry of Education and Research (BMBF) via the grant iCross—integrity of nuclear waste repositories, cross-scale system understanding and analysis (grant to H-HR)—and the Helmholtz Association of German Research Centres. The ProVis platform is financed by the European Regional Development Funds (EFRE–Europe funds Saxony) and the Helmholtz Association.

Acknowledgments

We acknowledge Jasmin Voigt for the technical support as well as Moritz Kuhner for his participation to this project. We acknowledge the ProVis platform at the Helmholtz Centre for Environmental Research–UFZ for sharing their analytical facilities.

Conflict of interest

H-HR is a guest scientist and hold stakes of Isodetect.

The remaining authors declare that the research was conducted in the absence of any commercial or financial relationships that could be construed as a potential conflict of interest.

The authors FM, HHR and CV declared that they were editorial board members of Frontiers, at the time of submission. This had no impact on the peer review process and the final decision.

Publisher's note

Supplementary material

The Supplementary Material for this article can be found online at: https://www.frontiersin.org/articles/10.3389/fgeoc.2023.1244283/full#supplementary-material

References

Albahri, M. B., Barifcani, A., Iglauer, S., Lebedev, M., O'Neil, C., Salgar-Chaparro, S. J., et al. (2021). Investigating the mechanism of microbiologically influenced corrosion of carbon steel using X-ray micro-computed tomography. *J. Mat. Sci.* 56, 13337–13371. doi:10.1007/s10853-021-06112-9

Ayala-Luis, K. B., Koch, C. B., and Hansen, H. C. B. (2008). The standard gibbs energy of formation of Fe(II)Fe(III) hydroxide sulfate green rust. *Clays Clay Min.* 56, 633–644. doi:10.1346/CCMN.2008.0560604

Azoulay, I., Rémazeilles, C., and Refait, P. (2012). Determination of standard Gibbs free energy of formation of chukanovite and Pourbaix diagrams of iron in carbonated media. *Corros. Sci.* 58, 229–236. doi:10.1016/j.corsci.2012.01.033

Bagnoud, A., Chourey, K., Hettich, R. L., De Bruijn, I., Andersson, A. F., Leupin, O. X., et al. (2016). Reconstructing a hydrogen-driven microbial metabolic network in Opalinus Clay rock. *Nat. Commun.* 7, 2770–2780. doi:10.1038/ncomms12770

Bénézeth, P., Dandurand, J. L., and Harrichoury, J. C. (2009). Solubility product of siderite (FeCO3) as a function of temperature (25-250 °C). *Chem. Geol.* 265, 3–12. doi:10.1016/j.chemgeo.2009.03.015

Birkholzer, J., Houseworth, J., and Tsang, C. F. (2012). Geologic disposal of high-level radioactive waste: status, key issues, and trends. *Annu. Rev. Environ. Resour.* 37, 79–106. doi:10.1146/annurev-environ-090611-143314

Cord-Ruwisch, R. (1985). A quick method for the determination of dissolved and precipitated sulfides in cultures of sulfate-reducing bacteria. *J. Microbiol. Methods* 4, 33–36. doi:10.1016/0167-7012(85)90005-3

Csákberényi-Malasics, D., Rodriguez-Blanco, J. D., Kis, V. K., Rečnik, A., Benning, L. G., and Pósfai, M. (2012). Structural properties and transformations of precipitated FeS. *Chem. Geol.* 294–295, 249–258. doi:10.1016/j.chemgeo.2011.12.009

Das, S., and Hendry, M. J. (2011). Application of Raman spectroscopy to identify iron minerals commonly found in mine wastes. *Chem. Geol.* 290, 101–108. doi:10.1016/j.chemgeo.2011.09.001

De La Pierre, M., Carteret, C., Maschio, L., André, E., Orlando, R., and Dovesi, R. (2014). The Raman spectrum of CaCO3 polymorphs calcite and aragonite: a combined experimental and computational study. *J. Chem. Phys.* 140, 164509. doi:10.1063/1.4871900

Deng, D., Zhang, L., Dong, M., Samuel, R., Ofori-Boadu, A., and Lamssali, M. (2020). Radioactive waste: a review. *Water Environ. Res.* 92, 1818–1825. doi:10.1002/wer.1442

Dinh, H. T., Kuever, J., Mußmann, M., Hassel, A. W., Stratmann, M., and Widdel, F. (2004). Iron corrosion by novel anaerobic microorganisms. *Nature* 427, 829–832. doi:10.1038/nature02321

Engel, K., Ford, S. E., Coyotzi, S., McKelvie, J., Diomidis, N., Slater, G., et al. (2019). Stability of microbial community profiles associated with compacted bentonite from the grimsel underground research laboratory. *mSphere* 4, e00601-19–e00610. doi:10.1128/msphere.00601-19

Enning, D., and Garrelfs, J. (2014). Corrosion of iron by sulfate-reducing bacteria: new views of an old problem. *Appl. Environ. Microbiol.* 80, 1226–1236. doi:10.1128/AEM.02848-13

Enning, D., Venzlaff, H., Garrelfs, J., Dinh, H. T., Meyer, V., Mayrhofer, K., et al. (2012). Marine sulfate-reducing bacteria cause serious corrosion of iron under electroconductive biogenic mineral crust. *Environ. Microbiol.* 14, 1772–1787. doi:10.1111/j.1462-2920.2012.02778.x

GNS (2023). Pollux. Available at: https://www.gns.de/language=de/24376/pollux (Accessed June 2023, 21).

Gu, B., Watson, D. B., Wu, L., Phillips, D. H., White, D. C., and Zhou, J. (2002). Microbiological characteristics in a zero-valent iron reactive barrier. *Environ. Monit. Assess.* 77, 293–309. doi:10.1023/A:1016092808563

Gutierrez, O., Park, D., Sharma, K. R., and Yuan, Z. (2009). Effects of long-term ph elevation on the sulfate-reducing and methanogenic activities of anaerobic sewer biofilms. *Water Research* 43, 2549–2557. doi:10.1016/j.watres.2009.03.008

Herbert, R. B., Benner, S. G., Pratt, A. R., and Blowes, D. W. (1998). Surface chemistry and morphology of poorly crystalline iron sulfides precipitated in media containing sulfate-reducing bacteria. *Chem. Geol.* 144, 87–97. doi:10.1016/S0009-2541(97)00122-8

Hoffmann, T. D., Reeksting, B. J., and Gebhard, S. (2021). Bacteria-induced mineral precipitation: a mechanistic review. *Microbiology* 167, 001049–001052. doi:10.1099/mic.0.001049

Hope, G. A., Woods, R., and Munce, C. G. (2001). Raman microprobe mineral identification. *Miner. Eng.* 14, 1565–1577. doi:10.1016/s0892-6875(01)00175-3

Hua, G., and Li, D. (2011). Generic relation between the electron work function and Young's modulus of metals. *Appl. Phys. Lett.* 99, 1–4. doi:10.1063/1.3614475

Iacoviello, F., Cocco, V. D., and Favaro, G. (2018). Pearlitic Ductile Cast Iron: mechanical properties gradient analysis in graphite elements. *Procedia Struct. Integr.* 9, 9–15. doi:10.1016/j.prostr.2018.06.004

Kim, J. S., Kwon, S. K., Sanchez, M., and Cho, G. C. (2011). Geological storage of high level nuclear waste. *KSCE J. Civ. Eng.* 15, 721–737. doi:10.1007/s12205-011-0012-8

King, F. (2017). "Nuclear waste canister materials: corrosion behavior and long-term performance in geological repository systems," in *Geological repository systems for safe disposal of spent nuclear fuels and radioactive waste*. Editors M. J. Apted, and J. Ahn (Elsevier Ltd), 365–408.

Langer, M. (1999). Principles of geomechanical safety assessment for radioactive waste disposal in salt structures. *Eng. Geol.* 52, 257–269. doi:10.1016/s0013-7952(99)00010-1

Laso-Pérez, R., Krukenberg, V., Musat, F., and Wegener, G. (2018). Establishing anaerobic hydrocarbon-degrading enrichment cultures of microorganisms under strictly anoxic conditions. *Nat. Protoc.* 13, 1310–1330. doi:10.1038/nprot.2018.030

Masurat, P., Eriksson, S., and Pedersen, K. (2010a). Evidence of indigenous sulphate-reducing bacteria in commercial Wyoming bentonite MX-80. *Appl. Clay Sci.* 47, 51–57. doi:10.1016/j.clay.2008.07.002

Masurat, P., Eriksson, S., and Pedersen, K. (2010b). Microbial sulphide production in compacted Wyoming bentonite MX-80 under *in situ* conditions relevant to a repository for high-level radioactive waste. *Appl. Clay Sci.* 47, 58–64. doi:10.1016/j.clay.2009.01.004

McNeil, M. B., and Little, B. J. (1990). ***Technical note:***Mackinawite formation during microbial corrosion. *Corrosion* 46, 599–600. doi:10.5006/1.3585154

Mernagh, T. P., and Trudu, A. G. (1993). A laser Raman microprobe study of some geologically important sulphide minerals. *Chem. Geol.* 103, 113–127. doi:10.1016/0009-2541(93)90295-T

Ning, J., Zheng, Y., Young, D., Brown, B., and Nešić, S. (2014). Thermodynamic study of hydrogen sulfide corrosion of mild steel. *Corrosion* 70, 375–389. doi:10.5006/0951

Pereira, A., Costa, M., Anflor, C., Pardal, J., and Leiderman, R. (2018). Estimating the effective elastic parameters of nodular cast iron from micro-tomographic imaging and multiscale finite elements: comparison between numerical and experimental results. *Met. (Basel)* 8, 695–708. doi:10.3390/met8090695

Punburi, P., Tareelap, N., Srisukhumbowornchai, N., Euaruksakul, C., and Yordsri, V. (2018). Correlation between electron work functions of multiphase Cu-8Mn-8Al and de-alloying corrosion. *Appl. Surf. Sci.* 439, 1040–1046. doi:10.1016/j.apsusc.2018.01.018

Rabus, R., Venceslau, S. S., Wöhlbrand, L., Voordouw, G., Wall, J. D., and Pereira, I. A. C. (2015). A post-genomic view of the ecophysiology, catabolism and biotechnological relevance of sulphate-reducing prokaryotes. *Adv. Microb. Physiology* 66, 55–321. doi:10.1016/bs.ampbs.2015.05.002

Rémazeilles, C., Saheb, M., Neff, D., Guilminot, E., Tran, K., Bourdoiseau, J. A., et al. (2010). Microbiologically influenced corrosion of archaeological artefacts: characterisation of iron(II) sulfides by Raman spectroscopy. *J. Raman Spectrosc.* 41, 1425–1433. doi:10.1002/jrs.2717

Rickard, D. (2014). The sedimentary sulfur system: biogeochemistry and evolution through geologic time. *Treatise Geochem.*, 267–326. doi:10.1016/b978-0-08-095975-7.00710-5

Rosner, B. (1975). On the detection of many outliers. *Technometrics* 17, 221–227. doi:10.2307/1268354

Saheb, M., Neff, D., Bellot-Gurlet, L., and Dillmann, P. (2010). Raman study of a deuterated iron hydroxycarbonate to assess long-term corrosion mechanisms in anoxic soils. *J. Raman Spectrosc.* 42, 1100–1108. doi:10.1002/jrs.2828

Simonov, P., and Likholobov, V. (2003). "Physicochemical aspects of preparation of carbon-supported noble metal catalysts," in *Catalysis and electrocatalysis at nanoparticle surfaces*. Editors A. Wieckowski, A. R. Savinova, and C. G. Vayenas (Boca Raton: Taylor and Francis), 409–454.

Smith, P., Poller, A., Mayer, G., and Hayek, M. (2014). *Technical report 14-09*. Wettingen: Nagra. No: ISSN 1015-2636.

Speich, G., Schwoeble, A. J., and Kapadia, B. M. (1980). Elastic moduli of gray and nodular cast iron. *J. Appl. Mech.* 47, 821–826. doi:10.1115/1.3153797

Stroes-Gascoyne, S., Hamon, C. J., Maak, P., and Russell, S. (2010). The effects of the physical properties of highly compacted smectitic clay (bentonite) on the culturability of indigenous microorganisms. *Appl. Clay Sci.* 47, 155–162. doi:10.1016/j.clay.2008.06.010

Stroes-Gascoyne, S., Hamon, C. J., and Maak, P. (2011). Limits to the use of highly compacted bentonite as a deterrent for microbiologically influenced corrosion in a nuclear fuel waste repository. *Phys. Chem. Earth, Parts A/B/C* 36, 1630–1638. doi:10.1016/j.pce.2011.07.085

Tamisier, M., Schmidt, M., Vogt, C., Kümmel, S., Stryhanyuk, H., Musat, N., et al. (2022). Iron corrosion by methanogenic archaea characterized by stable isotope effects and crust mineralogy. *Environ. Microbiol.* 24, 583–595. doi:10.1111/1462-2920.15658

Thibeau, R. J., Brown, C. W., and Heidersbach, R. H. (1978). Raman spectra of possible corrosion products of Iron. *Appl. Spectrosc.* 32, 532–535. doi:10.1366/000370278774330739

Tran, T. T. T., Kannoorpatti, K., Padovan, A., and Thennadil, S. (2021). Effect of pH regulation by sulfate-reducing bacteria on corrosion behaviour of duplex stainless steel 2205 in acidic artificial seawater. *R. Soc. Open Sci.* 8, 200639–200652. doi:10.1098/rsos.200639

Venzlaff, H., Enning, D., Srinivasan, J., Mayrhofer, K. J. J., Hassel, A. W., Widdel, F., et al. (2013). Accelerated cathodic reaction in microbial corrosion of iron due to direct electron uptake by sulfate-reducing bacteria. *Corros. Sci.* 66, 88–96. doi:10.1016/j.corsci.2012.09.006

Widdel, F. (2010). "Cultivation of anaerobic microorganisms with hydrocarbons as growth substrates," in *Handbook of hydrocarbon and lipid microbiology*. Editor K. N. Timmis (Berlin, Heidelberg: Springer), 3787–3798.

Zhang, Q., Zheng, M., Huang, Y., Kunte, H. J., Wang, X., Liu, Y., et al. (2019). Long term corrosion estimation of carbon steel, titanium and its alloy in backfill material of compacted bentonite for nuclear waste repository. *Sci. Rep.* 9, 3195–3213. doi:10.1038/s41598-019-39751-9